CSIRO PUBLISHING
www.publish.csiro.au/journals/ijwf International Journal of Wildland Fire, 2005, 14, 61–75

Coherent vortical structures in numerical simulations of buoyant plumes from wildland fires

Philip Cunningham[A,E], *Scott L. Goodrick*[B], *M. Yousuff Hussaini*[C] *and Rodman R. Linn*[D]

[A]Department of Meteorology and Geophysical Fluid Dynamics Institute, The Florida State University, Tallahassee, FL 32306, USA.
[B]USDA Forest Service, Southern Research Station, Athens, GA 30603, USA.
[C]School of Computational Science and Information Technology, The Florida State University, Tallahassee, FL 32306, USA.
[D]Earth and Environmental Sciences Division, Los Alamos National Laboratory, Los Alamos, NM 87545, USA.
[E]Corresponding author. Telephone: +1 850 644 4334; fax: +1 850 644 9642; email: cunningham@met.fsu.edu

Abstract. The structure and dynamics of buoyant plumes arising from surface-based heat sources in a vertically sheared ambient atmospheric flow are examined via simulations of a three-dimensional, compressible numerical model. Simple circular heat sources and asymmetric elliptical ring heat sources that are representative of wildland fires of moderate intensity are considered. Several different coherent vortical structures that dominate the plume structure and evolution are evident in the simulations, and these structures correspond well with those observed in plumes from wildland fires. For the circular source, these structures include: (i) a counter-rotating vortex pair aligned with the plume trajectory that is associated with a bifurcation of the plume, (ii) transverse shear-layer vortices on the upstream face of the plume, and (iii) vertically oriented wake vortices that form periodically with alternating sign on either side of the downstream edge of the plume base. For the elliptical ring source, a streamwise counter-rotating vortex pair is apparent on each flank, and a transverse horizontal vortex is observed above the head of the source. In all simulations the plume cross section is represented poorly by a self-similar Gaussian distribution.

Introduction

Plumes from wildfires and prescribed fires represent a critical aspect of smoke management, and as such an accurate prediction of plume rise and dispersion is critical for air quality assessment purposes. To develop such accurate predictions, it is important to unravel the basic mechanisms underlying the dynamics of buoyant plumes due to intense surface heat sources over a wide range of atmospheric conditions (i.e. wind and temperature profiles).

Many current models employed for the prediction of plume rise are so-called 'integral models', which assume self-similar cross-sectional profiles of physical quantities, typically of Gaussian structure, along the centre line of the plume, together with simple laws describing the entrainment of ambient air into the plume. Development of these models largely follows the analysis of Morton *et al.* (1956), extended to include the effects of neutral and stably stratified cross flows (e.g. Slawson and Csanady 1967; Briggs 1975; Weil 1988). Integral models may provide accurate predictions of the plumes arising from low-intensity fires; however, they are frequently inadequate for describing the behaviour of plumes originating from fires of higher intensity, particularly those with complex spatial configurations. In such fires, the dynamical interaction between the buoyancy-generated vorticity in the plume and the vorticity in the ambient atmosphere may be significant, and the behaviour of the plume may differ substantially from the predictions of the integral models, possibly dramatically so in the region near the fire.

These plumes are typically dominated by coherent vortex structures of varying size and nature that control the evolution of the flow. In this regard, buoyant plumes in a cross flow appear to share many common properties with non-buoyant jets in a cross flow, which have been studied much more extensively (for a review, see Margason 1993). Several types of vortices have been identified in such flows, and these are illustrated schematically in Fig. 1. The dominant feature in these flows is typically the counter-rotating vortex pair, which is observed in the far field aligned with the jet or plume

10.1071/WF04044 1049-8001/05/010061

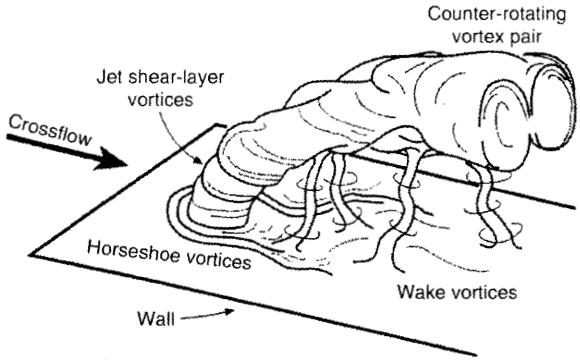

Fig. 1. Schematic illustration depicting four types of vortical structures associated with a non-buoyant jet in a cross flow: jet shear-layer vortices at the perimeter of the bending jet; the counter-rotating vortex pair; horseshoe vortices on the wall; and wake vortices extending from the wall to the jet. From Fric and Roshko (1994).

trajectory; this vortex pair is manifested as an approximately kidney-shaped cross section for scalar concentration, and in extreme cases can result in the split, or bifurcation, of the jet or plume some distance downstream of the source. Observations of plume bifurcation in association with intense ground fires are relatively common (Church *et al.* 1980; Haines and Smith 1987; Banta *et al.* 1992; McGrattan *et al.* 1996), although a visible bifurcation is often short lived, possibly due to mixing by ambient atmospheric turbulence.

While the counter-rotating vortex pair is apparently a ubiquitous feature of jets in a cross flow, and might thus be expected to be so for plumes also, there is still considerable debate about its generation and evolution (e.g. Coelho and Hunt 1989; Morton and Ibbetson 1996; Yuan and Street 1998; Yuan *et al.* 1999; Cortelezzi and Karagozian 2001; Lim *et al.* 2001). Nevertheless, there is a general consensus in the contemporary literature that in non-buoyant jets this feature arises as a consequence of the interaction between the cross-flow boundary layer and the jet shear layer. For plumes in a cross flow, the presence of buoyancy may further complicate the description. The existence of a kidney-shaped, or possibly bifurcated, structure for the plume cross section might also call into question the common practice of using Gaussian profiles for plume cross-section structure (Janseen *et al.* 1990), although it is possible that at large distances from the source, where buoyancy generated turbulence in the plume is comparable to ambient turbulence in the atmosphere, a Gaussian distribution may be appropriate. It is also possible that the time-averaged plume cross section structure might be close to Gaussian.

The wake vortices depicted in Fig. 1 and studied experimentally by Fric and Roshko (1994) for jets in a cross flow also have a counterpart in buoyant windblown plumes. Specifically, vertically oriented vortices bearing a strong resemblance to dust devils, or even tornadoes, have frequently been observed downwind of intense fires (Church *et al.* 1980; McRae and Flannigan 1990; Soma and Saito 1991; Wood 1992), extending from the ground to the underside of the bent-over plume. Occasionally, such vortices pass over and entrain burning material, resulting in a so-called fire whirl with an internal flame that can reach heights of tens of meters.

Although jets in a cross flow have been the subject of many numerical investigations (see Yuan *et al.* (1999), Cortelezzi and Karagozian (2001), and references therein), with notable exceptions there have been relatively few numerical simulation studies of buoyant plumes in a cross flow. To date, the majority of numerical investigations in this regard have been either two-dimensional (Luti 1980, 1981; Heilman and Fast 1992; Porterie *et al.* 1999) or quasi-three-dimensional, in which the streamwise velocity is taken to be constant, and the governing equations are solved in planes perpendicular to the streamwise direction (Zhang and Ghoniem 1993; McGrattan *et al.* 1996; Trelles *et al.* 1999). Although these studies have yielded significant insight into the structure and dynamics of buoyant plumes, and the quasi-three-dimensional models are able to represent the counter-rotating vortex pair, none of these models can represent fully the evolving three-dimensional vorticity. More recently, Baum and McGrattan (2000) have performed three-dimensional large-eddy simulations of plumes from outdoor industrial fires; however, the three-dimensional vortical structures evident in their simulated plumes were not the primary focus of their study.

The present study represents our preliminary attempts to simulate buoyant plumes arising from wildland fires in the presence of a cross flow using a fully three-dimensional numerical model. Of particular interest in this regard is whether the model is capable of capturing the vortical structures described above, and the dependence of these structures on physical and numerical parameters. Also of interest is the extent to which the simulated plumes demonstrate similarities or differences with the predictions of the simple integral models. The numerical model is based on the three-dimensional, compressible Navier–Stokes equations including heat source and surface drag terms, and is solved using direct and large-eddy simulation techniques. These simulations are employed to examine the effect of vertical wind shear near the surface, and of heat-source shape and intensity, on buoyant plumes arising from heat sources on the ground.

In the next section, the numerical model to be employed in this study is described, along with the form of the heat sources that will be used. In the subsequent two sections, results are presented from simulations using respectively a simple circular heat source and a heat source with spatial structure more representative of a wildland fire. In the final section, a summary of the primary results of the present study is presented, along with a discussion of the relevance of the results to the behaviour of buoyant plumes in general.

Model formulation and solution technique

We consider the ambient atmospheric wind profile to be an initially laminar flow, $U(z)$, in the positive x-direction as follows:

$$U(z) = U_0 \tanh(z/z_0) \tag{1}$$

where $U_0 = 4.5\ \mathrm{m\,s^{-1}}$, and z_0 is varied in an effort to understand the impact on plume dynamics of vertical wind shear near the surface. The specification of a laminar cross flow is consistent with the goal of this investigation of developing a basic understanding of the dynamics of the plume, but it also has a physical basis in the assumption that the turbulence generated by the plume is expected to be significantly larger in magnitude than the ambient atmospheric turbulence. For moderate to intense heat sources, this assumption would appear to be reasonable within 1 or 2 km from the fire. Nevertheless, the effects of ambient atmospheric turbulence on plume rise and dispersion are important for practical prediction, and will be addressed in future work.

Governing equations

The governing equations are those for three-dimensional, compressible flow in a density-stratified atmosphere forced by a prescribed volumetric heat source, Q:

$$\frac{\partial}{\partial t}(\rho u_i) + \frac{\partial}{\partial x_j}(\rho u_i u_j) + \frac{\partial p'}{\partial x_i} - g\rho'\delta_{i3} = \frac{\partial \tau_{ij}}{\partial x_j} - D_i, \tag{2}$$

$$\frac{\partial}{\partial t}(\rho\theta) + \frac{\partial}{\partial x_j}(\rho\theta u_j) = \frac{\partial}{\partial x_j}\left(\frac{k}{c_p}\frac{\partial \theta}{\partial x_j}\right) + \frac{Q\theta}{c_p T}, \tag{3}$$

$$\frac{\partial \rho}{\partial t} + \frac{\partial}{\partial x_j}(\rho u_j) = 0, \tag{4}$$

where ρ is the density, u_i is the wind velocity in the x_i direction with $i, j, k = 1$, 2, or 3 representing streamwise (x), spanwise (y), or vertical (z) directions, respectively, p' and ρ' are the departures of pressure and density, respectively, from a hydrostatic base state, D_i is a drag term, θ is the potential temperature, T is the temperature, c_p is the specific heat at constant pressure, and k is the thermal conductivity. The stress tensor, τ_{ij}, is given by

$$\tau_{ij} = \mu\left(\frac{\partial u_i}{\partial x_j} + \frac{\partial u_j}{\partial x_i}\right) - \frac{2}{3}\mu\frac{\partial u_k}{\partial x_k}\delta_{ij}, \tag{5}$$

where μ is the viscosity. Finally, the drag term, D_i, is intended to represent the effects of a vegetation canopy, and is defined as

$$D_i = \rho C_d a V u_i, \tag{6}$$

where C_d is the canopy drag coefficient, a is the canopy density, and V is the magnitude of the wind speed parallel to the ground. More generally, this term can be used to represent a rough lower boundary in simulations of the atmospheric boundary layer; Brown *et al.* (2001) show that the use of a canopy drag term identical to equation (6) in large-eddy simulations of a neutral boundary layer led to a significantly improved representation of logarithmic mean wind profiles in the near-surface region over those predicted by a traditional wall stress modelling approach. In this paper, we choose $C_d = 0.1$ and $a = 0.25\ \mathrm{m^{-1}}$ on the lowest grid level and zero elsewhere. It should be noted, however, that no extensive testing has been performed regarding the choice of these parameters, and further work is required to assess the optimal values and distributions in this regard.

In this paper, we employ two numerical approaches to solving the governing equations: the first is based on a direct approach to simulating the equations, whereas the second is based on large-eddy simulation (LES) methods. In the direct approach, it is assumed that the important energy-containing features are resolved on the grid and that no subgrid-scale model is required. Although such simulations are restricted to Reynolds numbers that are much smaller than those typically found in the atmosphere, there is evidence to suggest that insight into many important aspects of high Reynolds number turbulence can indeed be obtained through direct simulations of low Reynolds number flows (e.g. Moeng and Rotunno 1990; Coleman 1999). Moreover, the absence of the uncertainty that may be introduced by the use of a subgrid-scale model lends clarity to the results of these simulations. Consequently, the primary goal of the direct approach to simulating the governing equations is to attempt to gain insight into the basic physical processes relevant to buoyant plumes in a cross flow, and how this behaviour depends qualitatively on the Reynolds number. In this approach, the viscosity and thermal conductivity assume constant 'molecular' values that are related via the Prandtl number,

$$\mathrm{Pr} = \frac{\mu c_p}{k}, \tag{7}$$

which is taken to be equal to 0.7.

For the LES, τ_{ij} is interpreted as a subgrid-scale stress tensor, and the viscosity and thermal conductivity are interpreted as subgrid-scale eddy coefficients that must be modeled. Since no well accepted approach currently exists for LES when large subgrid-scale gradients of buoyancy and temperature may be present, we adopt a conventional method that has been shown to be successful for buoyancy-dominated boundary layers (e.g. Deardorff 1973; Moeng and Wyngaard 1988) and acknowledge at this point that this approach may not be entirely appropriate. In this scheme, the eddy viscosity depends on the subgrid-scale turbulent kinetic energy, e, as follows

$$\mu = \rho C_k e^{1/2}\Delta, \tag{8}$$

where C_k is a constant and Δ is the grid spacing. The eddy conductivity is then related to the eddy viscosity via a turbulent Prandtl number of the form given by equation (7), which is assumed to be equal to 1/3 herein. To close the model,

an additional equation for the prediction of subgrid-scale turbulent kinetic energy is required, and is given by

$$\frac{\partial}{\partial t}(\rho e) + \frac{\partial}{\partial x_j}(\rho e u_j) = -\tau_{ij}\frac{\partial u_i}{\partial x_j} + 2\frac{\partial}{\partial x_j}\left(\mu\frac{\partial e}{\partial x_j}\right) - \frac{gk}{c_p\theta}\frac{\partial\theta}{\partial z} - \frac{\rho C_e e^{3/2}}{\Delta}, \quad (9)$$

where the last term on the right-hand side represents the dissipation of subgrid-scale turbulent kinetic energy. Following Moeng and Wyngaard (1988), values for the constants in equation (8) and equation (9) are chosen to be $C_k = 0.1$ and $C_e = 0.93$. It is important to note, however, that these numbers are empirically defined based on Kolmogorov inertial-subrange theory, and a variety of different values both for these constants and for the turbulent Prandtl number have been used by different investigators (e.g. Schumann 1991).

Finally, we note that the solution method, which is described below, exhibits numerical diffusion. Such diffusion is itself sometimes interpreted as an implicit turbulence model (e.g. Hussaini 1998; Margolin *et al.* 2002), although a clear theoretical foundation and detailed validation for such an approach is still lacking. Nevertheless, the diffusion provided by the numerical scheme is weak in comparison to the stress term for most of the simulations to be shown in this paper.

Form of the heat sources

In this initial attempt to simulate buoyant plumes from wildland fires, we assume for simplicity a form for the heat source in equation (3) that is of fixed spatial form, and constant in time after a brief (10 s) ramp-up period. A volumetric heat source is employed in an effort to represent heating due to a fire, with the total heat release rate chosen to be comparable to that expected in a wildland fire of moderate intensity. In future work, we will incorporate heat sources that evolve in a coupled manner with the atmosphere.

To explore the basic dynamics of plumes in a cross flow, a simple circular heat source is examined in the following section that has the form of a smoothed top-hat distribution:

$$Q(x,y,z,t) = \begin{cases} Q_0 \tanh(t/t_0)\exp(-z/h), & r < R_1, \\ Q_0 \tanh(t/t_0)\exp(-z/h) \\ \quad \times \left[\frac{1}{2} - \frac{1}{2}\tanh\left(\frac{r-R_c}{d}\right)\right], & R_1 \le r < R_2, \\ 0, & r \ge R_2, \end{cases} \quad (10)$$

where Q_0 is a constant that controls the intensity of the heat source, t_0 is the ramp-up time scale, h is the scale height, $r = [(x-x_h)^2 + (y-y_h)^2]^{1/2}$ is the horizontal distance from the centre of the heat source at $(x_h, y_h, 0)$, R_1 is the radius of the uniform heating area, R_2 is the radius of the total heating area, $R_c = (R_1 + R_2)/2$ and d is a scale width. For the simulations shown in this paper, we take $h = 25$ m, $x_h = 450$ m, $y_h = 600$ m, $R_1 = 75$ m, $R_2 = 150$ m, and $d = 12.5$ m.

Wildland fires rarely exhibit such simple configurations, however, and the maximum heat release is seldom located in the centre of the fire area. Typically, fires possess an asymmetric ring-like structure that is elliptical (with major axis in the streamwise direction), most intense at its forwards end (the head), less intense on the sides (the flanks), and weakest at its rear end (the back). Consequently, in this paper we also consider heat sources with shapes that are representative of this typical structure; specifically, the following functional form for the heat source is adopted:

$$Q(x,y,z,t) = Q_0 \tanh(t/t_0)\exp(-z/h) \times \left\{\frac{(\cos[\mathrm{atan}(Y/X)] + 1)}{2[2 - (X/A)^2 - (Y/B)^2]^4 + 2}\right\} \quad (11)$$

where $X = x - x_h$, $Y = y - y_h$, and we choose $A = 200$ m and $B = 100$ m such that the heat source assumes the form of an ellipse with major axis in the streamwise direction. All other parameters are the same as in equation (10). This heat source is referred to as the 'realistic' heat source. Horizontal distributions of the heat sources given by equation (10) and equation (11) are depicted in Fig. 2.

The total heat release rate associated with these sources is obtained by integrating the expressions for Q given in equation (10) and equation (11) over the volume in which Q is non-zero. For the smoothed top-hat source in equation (10), choosing $Q_0 = 1$ kW m^{-3} gives a total heat release rate of 1000 MW, and for the realistic source in equation (11), choosing $Q_0 = 1$ kW m^{-3} gives a total heat release rate of 1700 MW. Such values for the total heat release rate and the heat release per unit volume are considered representative of those found in typical wildland fires of moderate intensity.

Solution technique

To solve the governing equations described in the preceding sections, we use the Weather Research and Forecasting (WRF) model code (Skamarock *et al.* 2001). For time integration, a split-explicit method is employed that combines a third-order Runge–Kutta scheme for advection with a forwards–backward scheme for the high-frequency acoustic modes (Wicker and Skamarock 2002). Spatial discretization of the advection terms is treated via a fifth-order upwind-biased scheme.

The computational domain is depicted schematically in Fig. 3. The domain is a rectangular box with spatial dimensions $L_x \times L_y \times L_z$, where $L_x = 1800$ m, $L_y = 1200$ m, and $L_z = 1500$ m. A uniform grid spacing of 10 m is employed in all directions. At the lateral and downstream boundaries a non-reflecting outflow condition is prescribed (Orlanski

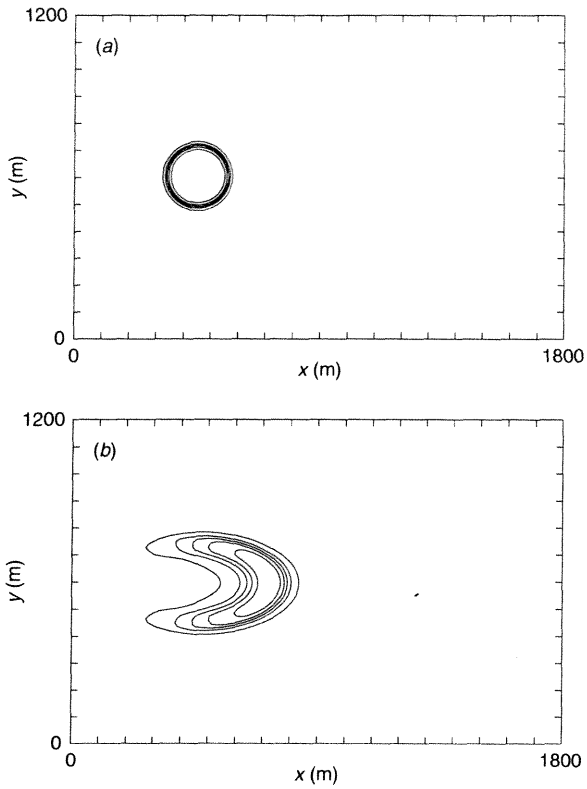

Fig. 2. Non-dimensional function for the spatial distribution of heating at the lowest model level for (*a*) the circular heat source and (*b*) the realistic heat source. Contours are for values between 0.1 and 0.9 with an interval of 0.2.

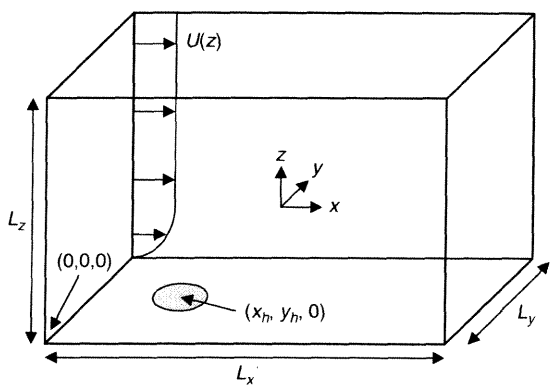

Fig. 3. Schematic illustration of the computational domain. The heat source, indicated by the shaded area, is centred at $(x_h, y_h, 0)$.

1976). At the upper and lower boundaries, solid-wall free-slip conditions are imposed; although such conditions are not optimal for models of the dimensions and spatial resolution used herein, it is noted that the upper boundary is high enough such that the outflow occurs entirely on the lateral and downstream boundaries of the domain. We have performed sensitivity experiments to ensure that the upper boundary has been placed sufficiently high that this choice has negligible effect on plume behavior. In addition, a layer of enhanced damping is placed adjacent to the upper boundary to avoid the reflection of energy back into the domain. At the lower boundary, the effects of the rough surface are treated via the drag term (equation 6). In all simulations, the ambient potential temperature is taken to be uniform and equal to 300 K.

Buoyant plumes from an idealized circular heat source

In this section, we describe simulations of the buoyant plumes arising from the heat source (equation 10) in the presence of the wind profile (equation 1). In an effort to gain basic insight into the laminar and turbulent structure of such plumes, several simulations using the direct approach have been performed with a range of different values of the viscosity, μ, keeping the Prandtl number fixed at 0.7. This approach is essentially equivalent to changing the Reynolds number of the simulation; however, given that there are several equally plausible ways to choose velocity and length scales for the plume in a cross flow, and since the model is not dimensionless, we do not define a specific Reynolds number for the present situations.

Figure 4 and Figure 5 show respectively the potential temperature and vorticity magnitude, $|\nabla \times \mathrm{V}|$, at $t = 1100$ s for four particular simulations with successively decreasing viscosity (increasing Reynolds number) as follows: $\mu = 4\,\mathrm{kg\,m^{-1}\,s^{-1}}$ (Figs 4*a*, 5*a*), $\mu = 1\,\mathrm{kg\,m^{-1}\,s^{-1}}$ (Figs 4*b*, 5*b*), $\mu = 0.15\,\mathrm{kg\,m^{-1}\,s^{-1}}$ (Figs 4*c*, 5*c*), and $\mu = 0.0015\,\mathrm{kg\,m^{-1}\,s^{-1}}$ (Figs 4*d*, 5*d*). For the large μ case, the plume is essentially laminar, and exhibits a well defined symmetric bifurcation (Fig. 4*a*). The corresponding vorticity field (Fig. 5*a*) clearly shows the associated counter-rotating vortex pair; however, no other vortical structures are apparent in this simulation. Near the surface the vertical component of vorticity in the pair is significant, with positive vorticity on the right-hand side looking downstream, and negative vorticity on the left-hand side, consistent with descriptions of observed plumes (e.g. Church *et al.* 1980). As μ is decreased (equivalent to increasing the nominal Reynolds number) the simulated plumes become turbulent and asymmetric, and additional vortical structures become evident. Nevertheless, the counter-rotating vortex pair remains a central, albeit unsteady, feature in all of the simulations, and the plume cross sections do not exhibit a self-similar Gaussian structure.

The transition to turbulence in these plumes appears to arise via the shear (i.e. Kelvin–Helmholtz) instability of the upstream face of the plume that leads to shear-layer vortices analogous to those seen in Fig. 1. Such a transition is apparent in Fig. 4*b* and Fig. 5*b* in which transverse vortices can be seen at the top of the laminar base of the plume; above

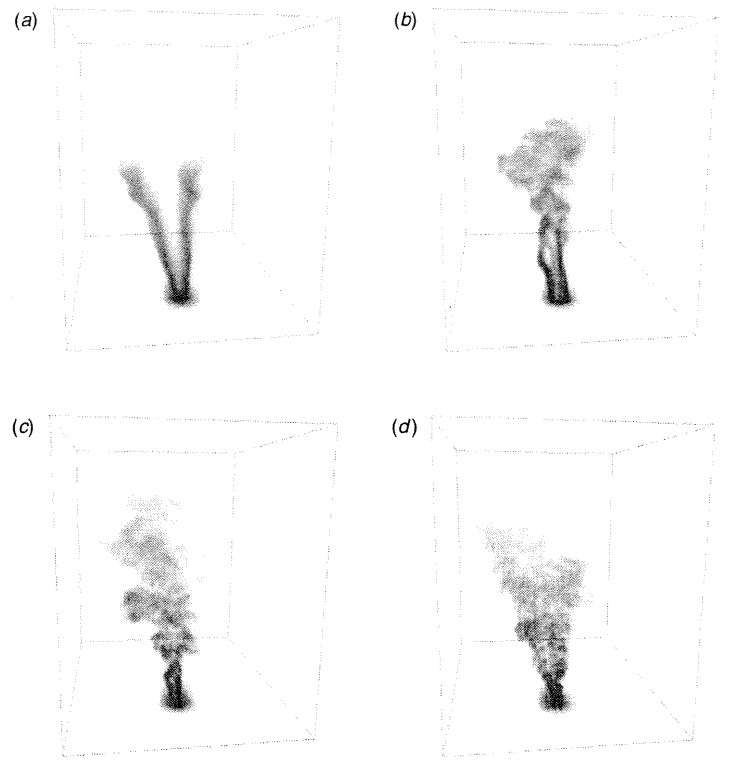

Fig. 4. Volume rendered potential temperature for the circular heat source simulations with: (*a*) $\mu = 4\,\mathrm{kg\,m^{-1}\,s^{-1}}$, (*b*) $\mu = 1\,\mathrm{kg\,m^{-1}\,s^{-1}}$, (*c*) $\mu = 0.15\,\mathrm{kg\,m^{-1}\,s^{-1}}$, and (*d*) $\mu = 0.0015\,\mathrm{kg\,m^{-1}\,s^{-1}}$. In all cases the view is looking downstream. Darker shades represent higher values of potential temperature.

these vortices the plume is turbulent. At the early stages of the lower Reynolds number simulations (not shown), the onset of this instability can be seen as a regularly spaced array of these transverse vortices, consistent with the low Reynolds number laboratory experiments of Perry and Lim (1978). Further decreases (increases) in the viscosity (Reynolds number) result first in the transition to turbulence occurring closer to the base of the plume (e.g. Figs 4*c*,*d*, 5*c*,*d*), and subsequently in the breakdown of the symmetric wake structure into an asymmetric one involving vertically oriented wake vortices. The view perspective in these figures does not provide an ideal illustration of the wake vortices, however, and these features are examined in further detail later in this section.

Before exploring the nature of vortical structures in the turbulent plumes, however, it is worthwhile to examine in more detail the low Reynolds number case in an attempt to gain additional insight into the dynamics of the counter-rotating vortex pair, which is a robust feature of all the simulations. Specifically, we explore the dependence of this feature on some of the parameters that define the present problem. To this end, six simulations were performed with $\mu = 4\,\mathrm{kg\,m^{-1}\,s^{-1}}$ for two different intensities for the heat source (i.e. $Q_0 = 1\,\mathrm{kW\,m^{-3}}$ and $0.5\,\mathrm{kW\,m^{-3}}$) and three different depths for the cross-flow shear layer (i.e. $z_0 = 50$ m, 100 m, and 150 m). Cross sections of potential temperature in the y–z plane at $x = 1750$ m for these simulations are shown in Fig. 6 for the time at which the flows are essentially steady (typically achieved after approximately 600 s). The principal result emerging from these simulations is that for larger z_0, which corresponds to a deeper cross-flow shear layer, the bifurcation of the plume is wider. Additionally, for a given cross flow, bifurcation is wider for the weak heat source than the strong heat source (compare Fig. 6*e* with Fig. 6*f*).

Based on this limited set of results we conjecture that, since the magnitude of the heat source is a major factor in the magnitude of the vertical velocity, the width of the bifurcation is controlled by the amount of time it takes for a buoyant parcel to rise through the shear layer. Presumably the relevant process is the entrainment and organized rearrangement of ambient horizontal vorticity in the cross-flow shear layer by the rising buoyant elements, although further investigation of the details of this process is necessary. A similar result will be shown in the simulations of the realistic heat source in the next section. It is important to note, however, that the presence and degree of bifurcation does not appear to impact the plume rise for a given heat source (e.g. compare Fig. 6*b*,*d*,*f*).

As discussed in the Introduction, the origin of the counter-rotating vortex pair in jets or plumes in a cross flow is still an unresolved issue, although it is generally accepted that this feature arises through an interaction between the vorticity

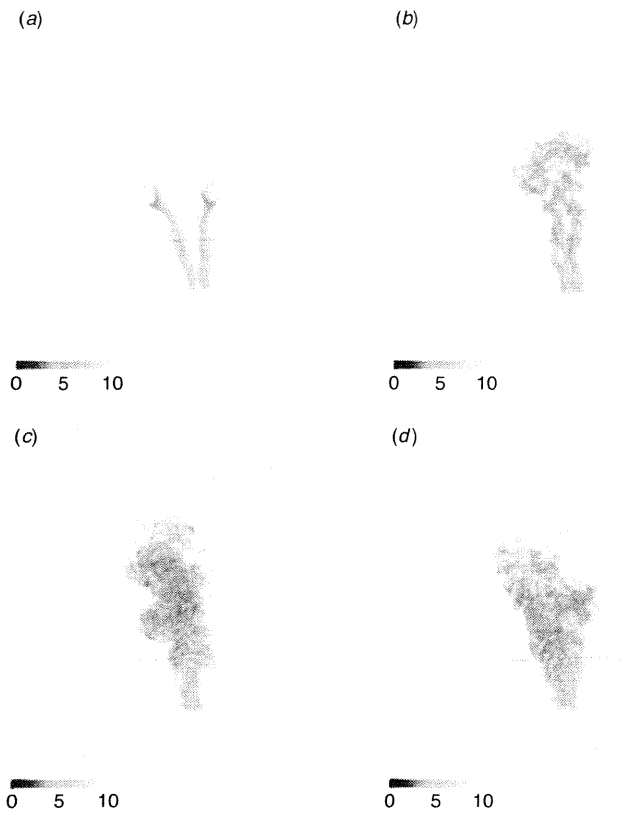

Fig. 5. Volume rendered vorticity magnitude (in s^{-1}, shaded as indicated) for the circular heat source simulations with: (*a*) $\mu = 4\,kg\,m^{-1}\,s^{-1}$, (*b*) $\mu = 1\,kg\,m^{-1}\,s^{-1}$, (*c*) $\mu = 0.15\,kg\,m^{-1}\,s^{-1}$, and (*d*) $\mu = 0.0015\,kg\,m^{-1}\,s^{-1}$. In all cases the view is looking downstream.

in the cross flow and the vorticity in the jet or plume. For the simulations shown here it is apparent that the counter-rotating vortex pair originates near the ground as a pair of vortices that are oriented primarily in the vertical direction (Fig. 5; see also Fig. 9 below). This result also appears to be true for non-buoyant jets in a cross flow (Yuan *et al.* 1999; Lim *et al.* 2001). It is important to note at this point that buoyancy can only directly generate horizontal vorticity, and that vertical vorticity can be generated only by tilting horizontal vorticity into the vertical direction; these are fundamental properties of the governing equations, not of the strength or distribution of the heat source. In this regard, in the absence of a cross flow the vorticity in a buoyant plume can be described in terms of horizontal vortex rings that propagate upwards. When a cross flow is present, the horizontal vorticity in the cross-flow shear layer is tilted upwards within these buoyant vortex rings, leading to a positive–negative couplet of vertical vorticity on the flanks of the plume. On the other hand, since the cross flow is horizontally uniform, there is no mechanism initially to tilt the horizontal vorticity of the plume, although once the cross-flow vorticity has been tilted into the vertical, the interaction becomes complex and three-dimensional.

In light of the foregoing discussion, we assert that the primary source of vorticity at the origin point of the counter-rotating vortex pair is the tilting of horizontal cross-flow vorticity into the vertical by the plume, since it is not obvious that the buoyancy-generated horizontal vorticity in the plume can be tilted into the vertical in such an organized fashion. Farther from the source in the bent-over region of the plume, however, the counter-rotating vortex pair is oriented primarily horizontally, and buoyancy may contribute directly to the vorticity in the counter-rotating vortex pair in the manner described by Zhang and Ghoniem (1993).

The foregoing simulations provide important insight into the basic dynamics of buoyant plumes in a cross flow, particularly with respect to the associated coherent vortical structures. As discussed previously, however, the direct approach to simulating the equations is restricted to low Reynolds number flows, and to simulate the high Reynolds numbers characteristic of the atmosphere, an explicit subgrid-scale model is required to represent small-scale turbulent mixing. Consequently, we continue our exploration into the dynamics of buoyant plumes in a cross flow using the LES version of the model, in which the turbulent mixing is parameterized as described in the previous section. For the remainder

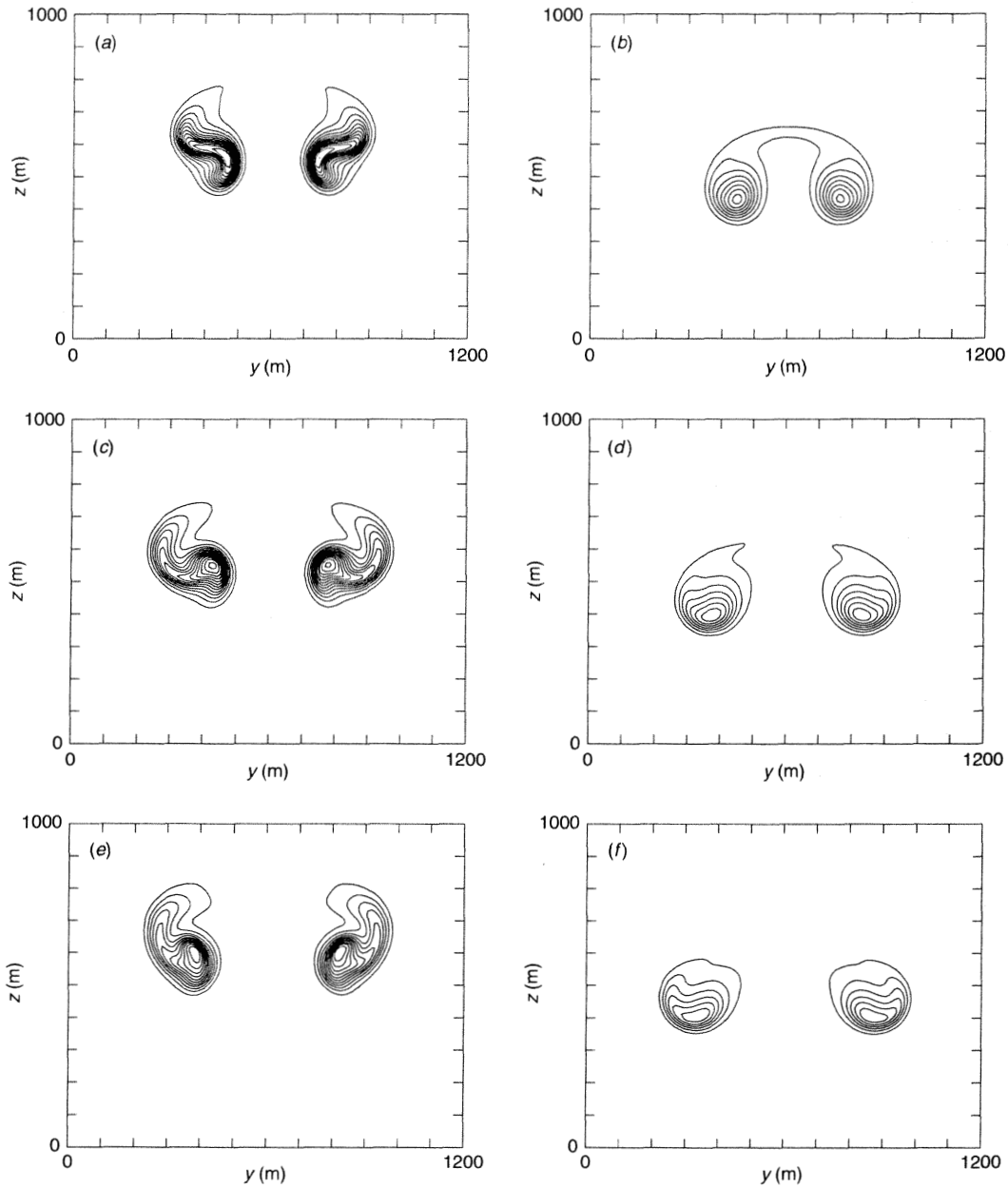

Fig. 6. Cross sections of potential temperature in the y–z plane at $x = 1750$ m for the circular heat source simulations ($\mu = 4\,\mathrm{kg\,m^{-1}\,s^{-1}}$) with $Q_0 = 1\,\mathrm{kW\,m^{-3}}$ (left column) for (*a*) $z_0 = 50$ m, (*c*) $z_0 = 100$ m, (*e*) $z_0 = 150$ m, and with $Q_0 = 0.5\,\mathrm{kW\,m^{-3}}$ (right column) for (*b*) $z_0 = 50$ m, (*d*) $z_0 = 100$ m, (*f*) $z_0 = 150$ m. Contour interval is 0.25 K with the first plotted contour equal to 300.25 K.

of this section, we focus on one specific simulation, namely for $Q_0 = 1\,\mathrm{kW\,m^{-3}}$ and $z_0 = 100$ m.

As with all other simulations, the counter-rotating vortex pair and the associated plume bifurcation are apparent throughout the evolution; however, in the present simulation these features undergo a quasi-periodic oscillation in which each branch of the pair is successively dominant over the other. This oscillation is illustrated in Fig. 7, in which it can be seen that at $t = 850$ s (Fig. 7*a*,*c*) the right-hand branch of the pair dominates, while at $t = 950$ s (Fig. 7*b*,*d*) the

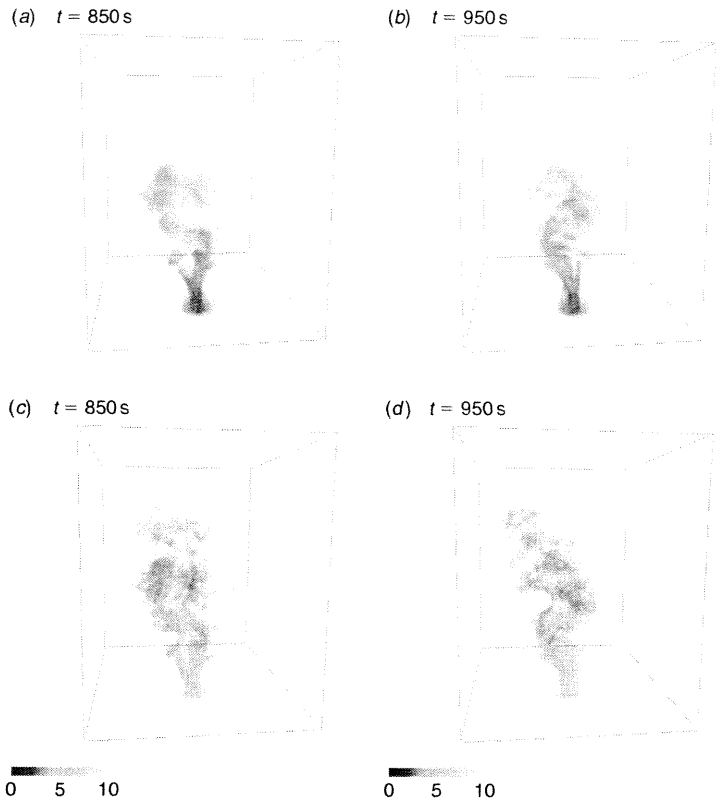

Fig. 7. Volume rendered potential temperature (darker shades represent higher values) at (*a*) $t = 850$ s and (*b*) $t = 950$ s, and vorticity magnitude (in s^{-1}, shaded as indicated) at (*c*) $t = 850$ s and (*d*) $t = 950$ s for the circular heat source LES.

left-hand branch dominates. To explore this oscillation further, we show in Fig. 8 the vertical component of vorticity within the cross-flow shear layer (at $z = 45$ m) for a range of times encompassing the oscillation of the plume seen in Fig. 7. It is readily apparent from this figure that there is a 'shedding' of localized regions of vertical vorticity with alternating sign from either side of the plume, with a period of about 200 s (note the similarity between Fig. 8*a* and Fig. 8*d*). This vertical vorticity corresponds to the wake vortices depicted in Fig. 1. The presence of a narrow turbulent wake downstream of the heat source near the surface is also apparent.

A non-dimensional number that has been shown to be relevant for the wake vortex system, both in non-buoyant jets in a cross flow (e.g. Fric and Roshko 1994) and in flow around a circular cylinder (e.g. Batchelor 1967), is the Strouhal number, defined by

$$\mathrm{St} = \frac{nD}{U_0}, \tag{12}$$

where n is the frequency of the oscillation, $D = 2R_c$ is the diameter of the heat source, and U_0 is the maximum cross flow speed. Based on an estimated period of 200 s, the Strouhal number in this case is approximately $\mathrm{St} = 0.25$. This value is comparable with that seen in experiments of the wake system in non-buoyant jets ($\mathrm{St} \approx 0.05$–0.2), and also for the wake vortices associated with flow around a solid cylinder ($\mathrm{St} \approx 0.2$), although it is stressed that the mechanism for the creation of the wake vortices is different for jets and plumes than it is for solid bodies, and the analogy of the plume as an obstacle in the flow is only partially accurate.

A graphic illustration of the wake vortices in this simulation is provided in Fig. 9, which shows the vertical component of vorticity for the same times as in Fig. 7. The successive formation of positive and negative vertical vortices downstream of the plume is readily apparent, as is their continued advection downstream. The 'positive phase' of the oscillation at $t = 850$ s, characterized by the creation of a positive vortex on the right-hand side of the plume (Fig. 9*a*), corresponds to the stage at which the plume is skewed to the right-hand side (Fig. 7*a*), while in the 'negative phase' at $t = 950$ s, the creation of a negative vortex on the left-hand side (Fig. 9*b*) corresponds to the plume being skewed to the left-hand side (Fig. 7*b*). The vortices are subsequently swept downstream and tilted away from the vertical by a combination of the plume and the cross flow.

It is important to note that the ability of the model to resolve the wake vortex system is a direct consequence of its three-dimensional nature. The quasi-three-dimensional models, in which the streamwise velocity is fixed (Zhang and

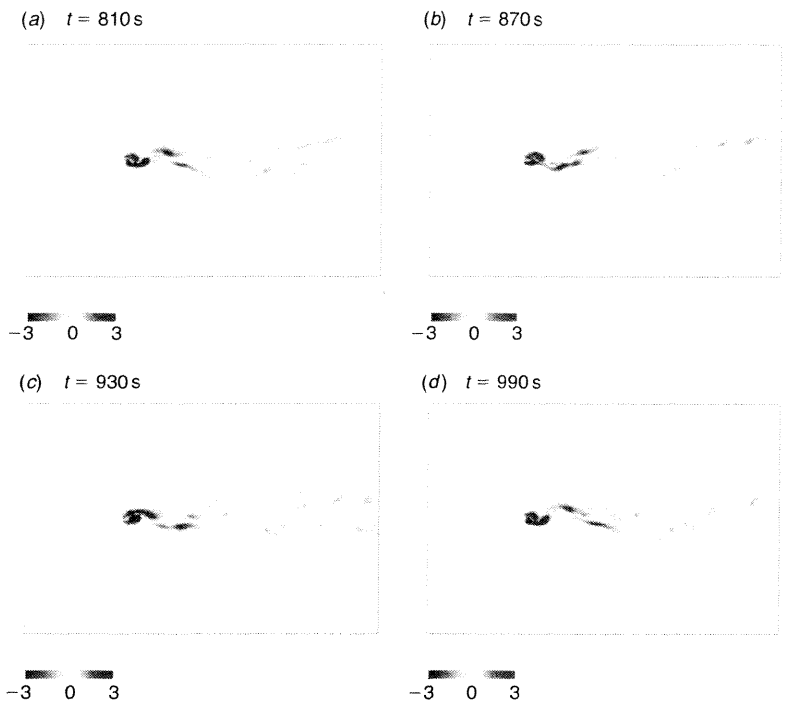

Fig. 8. Vertical component of vorticity (in s^{-1}, shaded as indicated) in the x–y plane at $z = 45$ m at (*a*) $t = 810$ s, (*b*) $t = 870$ s, (*c*) $t = 930$ s, and (*d*) $t = 990$ s for the circular heat source LES.

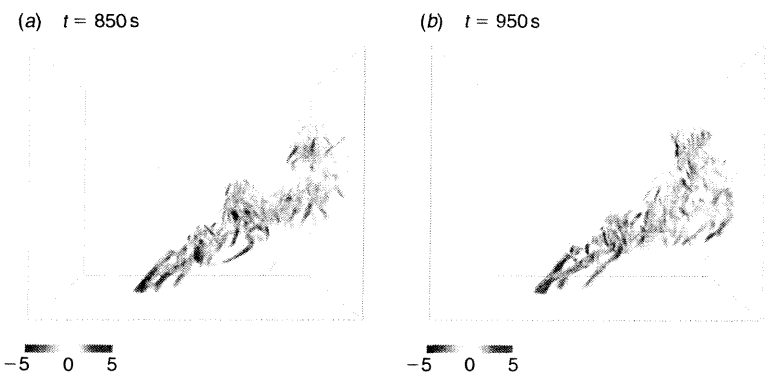

Fig. 9. Volume rendered vertical component of vorticity (in s^{-1}, shaded as indicated) at: (*a*) $t = 850$ s and (*b*) $t = 950$ s for the circular heat source LES.

Ghoniem 1993; McGrattan *et al.* 1996; Trelles *et al.* 1999), are able to treat only one of the three components of vorticity, namely the streamwise component. Consequently, these models are able to represent only the horizontal vorticity in the counter-rotating vortex pair. Nevertheless, since that is the dominant vortical structure in most buoyant plumes, these models are quite successful at predicting downwind plume concentrations, and they have the advantage over the present model that they can simulate larger downstream domains while using similar resolutions.

It is also noteworthy that the presence or absence of the wake vortex system depends on the effective Reynolds number of the simulations, and for low Reynolds numbers the wake region is essentially laminar and symmetric. The wake vortices are observed only for the higher Reynolds number direct simulations and the LES. We are unaware of any previously published results describing simulations of the wake vortex system for buoyant plumes in a cross flow; indeed, despite the large number of numerical studies of jets in a cross flow, simulations of the wake vortex system in that case are apparently also rare (e.g. Rudman 1996).

As a final note in this section, there was no apparent evidence in any of the simulations for the fourth vortical structure depicted in Fig. 1, namely the horseshoe vortex. This is not entirely surprising, however, since these features are almost entirely located within the cross-flow boundary layer

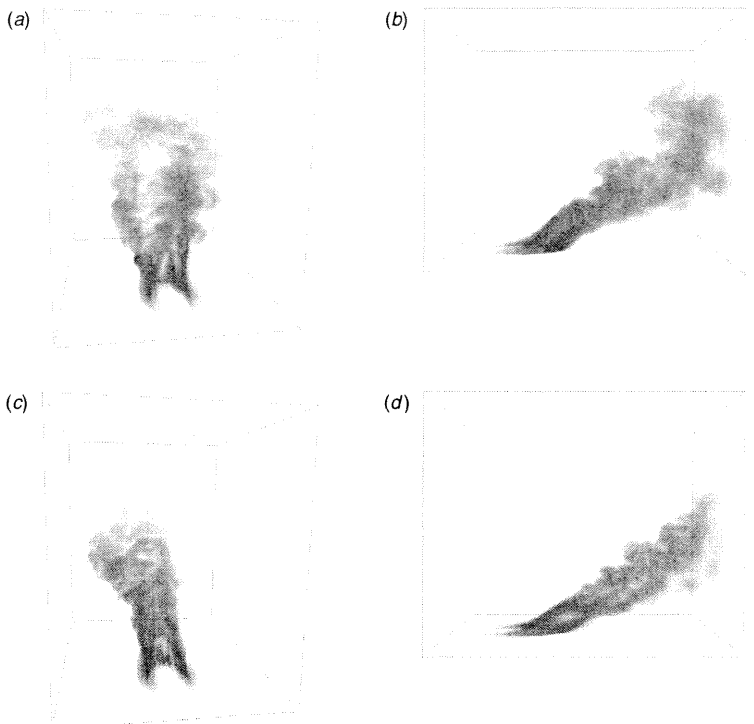

Fig. 10. Volume rendered potential temperature at $t = 1100$ s for the realistic heat source LES. The upper two images are for the deep shear layer (i.e. $z_0 = 150$ m) case with views from (*a*) the inflow boundary and (*b*) the lateral boundary. The lower two images are for the shallow shear layer (i.e. $z_0 = 50$ m) case with views in (*c*) and (*d*) identical to those in (*a*) and (*b*) respectively. Darker shades represent higher values of potential temperature.

and the resolution of the present simulations is inadequate to resolve the details of the near-surface flow.

Buoyant plumes from a heat source representative of a wildland fire

The preceding results demonstrate the ability of the model to reproduce the dominant features of buoyant plumes in a cross flow associated with circular heat sources. As noted previously, however, wildland fires represent a far more complex heat source with regions of heating that are essentially aligned in the streamwise direction (the fire flanks) and regions of heating that are aligned in the spanwise, or transverse, direction (the fire's head and back). The elliptical heat source depicted in Fig. 2*b* provides an idealized representation of a wildland fire with intensities increasing along the fires flanks towards the head. Using this heat source for cases with $z_0 = 50$ m and 150 m, referred to as shallow and deep shear layers, respectively, we employed the LES version of the model to examine its ability to simulate vortices associated with wildland fires as described by Haines and Smith (1987).

The first vortex type described by Haines and Smith was a horizontal vortex pair located along each fire flank. Figure 10 clearly shows the development of a dominant structure along each flank for both the deep (Fig. 10*a*) and the shallow (Fig. 10*c*) shear layers. While the transient nature of the flow renders the direct comparison of simultaneous instantaneous images from the two simulations rather difficult, the plume in the deep shear layer case maintains a more pronounced horizontal split between the structures of each flank than does that in the shallow shear layer case, consistent with the results shown in Fig. 6. The vertical spread of the plume at the downwind edge of the model domain is also greater for the deep shear layer; however, as with the bifurcated plumes in the circular heat source cases, the mean plume height is nearly identical for the two shear-layer depths (compare Fig. 10*b* with Fig. 10*d*).

The presence of counter-rotating vortex pairs along each flank is more clearly evident by viewing the vorticity field (Fig. 11). Vorticity maxima are located within the flanks of the fire, and examination of the vertical component of vorticity shows the counter-rotating nature of these vortices (Fig. 11*b*,*d*). Near the heat source the plume is composed of the dominant counter-rotating vortex pairs along each flank as well as smaller vortex pairs located along the fire perimeter. For the deep shear layer case, wake vortices are also evident just downstream of the heat source and extend from the underside of the bent-over plume down to the surface. As in the circular heat source case, positive vortices are preferred on the right-hand side downwind of the heat source, while negative vortices are preferred on the left-hand side. Wake vortices are not as obvious in the shallow shear layer case due to their transient nature; however, small and relatively

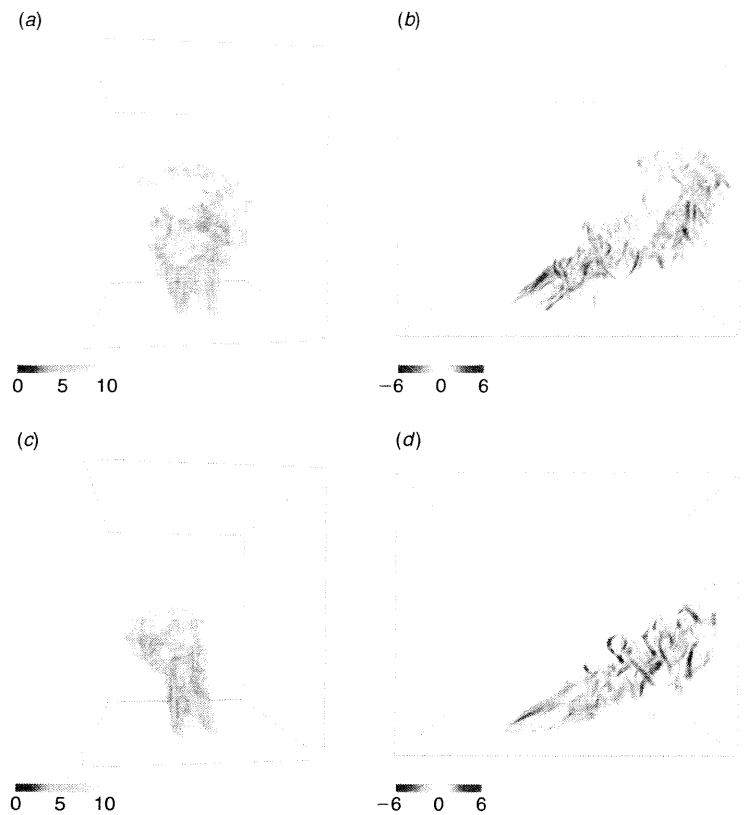

Fig. 11. Volume rendered vorticity magnitude (left column; in s^{-1}, shaded as indicated) and vertical component of vorticity (right column; in s^{-1}, shaded as indicated) at $t = 1100$ s for the realistic heat source LES for: (*a*) and (*b*) $z_0 = 150$ m; (*c*) and (*d*) $z_0 = 50$ m.

weak regions of vertical vorticity that are possible remnants of wake vortices are observed near the surface and downwind of the heat source.

The mechanism for producing the counter-rotating vortex pairs has been discussed in the previous section, and involves the interaction of the cross-flow shear-layer vorticity with the vorticity of the plume. However, it is to be expected that the details of this behavior may be significantly different for a spatially complex heat source. Examination of vortex lines at early stages of the shallow shear layer simulation (Fig. 12) reveal that the dominant counter-rotating vortex pairs along each fire flank are generated by the tilting of horizontal vorticity associated with the cross flow into the vertical to form loops in the vortex lines (Fig. 12*b*). As these loops are stretched in the vertical, the cross flow also acts to reorient them into streamwise vortices. As they near the head of the fire, however, the loop vortices from each flank begin to bend towards the region of most intense heating and become intertwined with the horizontal vorticity created by buoyancy at the head of the fire, creating an elevated horizontal vortex (Fig. 12*c*,*d*). This mechanism of concentrating horizontal vorticity at the head of fire may be analogous to the transverse vortices described by Haines and Smith (1987), since there appears to be some degree of periodicity to their formation, and they propagate along the underside of the plume. Nevertheless, more investigation of this phenomenon is required.

Using an idealized representation of a wildland fire as the heat source we were able to reproduce two of the three vortices observed by Haines and Smith (1987) in association with wildfires (longitudinal counter-rotating vortex pairs and the transverse vortex). The third vortex discussed by Haines and Smith (1987)—a single longitudinal vortex—is thought to require directional shear in the ambient flow, which was not included in the current simulations. In addition, Haines and Smith (1987) described the bifurcation of the smoke column, characterized by a separation of the counter-rotating vortex pairs along each flank, for a crown fire in Wisconsin (the New Miner Fire). The simulations presented here suggest that the depth of the shear layer may play a significant role in the bifurcation, since the plume is noticeably wider for the deep shear layer than for the shallow shear layer. The split column extends well outside the fire flanks and displays an oscillatory nature, and we hypothesize that this behavior may result in the plume dropping to the ground as observed in the New Miner Fire if either the shear layer was deeper or the ambient

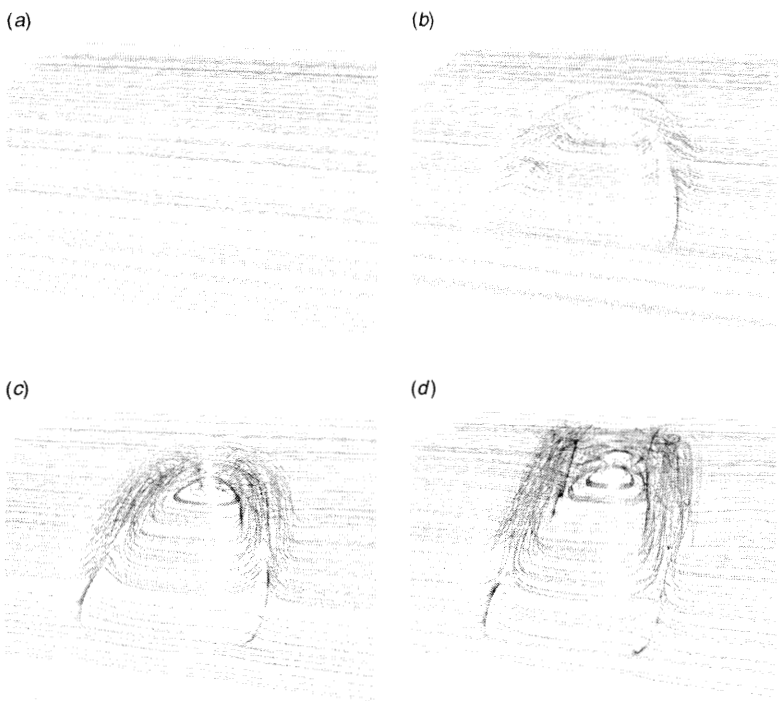

Fig. 12. Vortex lines and the $0.9\,s^{-1}$ isosurface of vorticity magnitude at (*a*) $t = 10$ s, (*b*) $t = 30$ s, (*c*) $t = 50$ s, and (*d*) $t = 70$ s for the realistic heat source LES with $z_0 = 50$ m.

stratification was unstable instead of neutral, as is the case for the present simulations. Exploring the possibility will be a subject of future simulations.

Summary and discussion

In this paper, we have described several three-dimensional numerical simulations of buoyant plumes arising from isolated, finite-area heat sources in the presence of a vertically sheared cross flow. The numerical model is based on the compressible Navier–Stokes equations and is solved using both direct and large-eddy simulation techniques in the framework of the Weather Research and Forecasting (WRF) model code (Skamarock *et al.* 2001), modified to include a volumetric heat source and surface drag. Two types of heat source were examined: (i) a simple circular (smoothed top-hat) heat source; and (ii) an asymmetric elliptical ring heat source—referred to as the 'realistic' heat source—that represents an idealization of a typical wildland fire, with intensities increasing along the fire flanks towards the head. Of particular interest in the present study was the extent to which the simulations were able to capture the variety of coherent vortical structures commonly seen, not just in wildland fires but more generally in buoyant plumes in a cross flow arising from a non-specific buoyancy forcing. These vortical structures control the turbulent mixing in the plume and, in the case of wildland fires, can potentially lead to erratic fire behavior if they are strong enough to interact with the fire (e.g. Haines and Smith (1987); see also the coupled atmosphere–fire simulations of Clark *et al.* (1996*a*, 1996*b*) and Linn *et al.* (2002)).

The plumes arising from circular heat sources in the presence of a cross flow exhibit many similarities with non-buoyant circular jets in a cross flow, particularly with respect to the types of coherent vortical structures present in these flows, although there are some differences related to the presence of buoyancy and the associated generation of horizontal vorticity. Specifically, the simulations presented herein were able to capture:

(1) The counter-rotating vortex pair aligned with the plume trajectory that is responsible for the bifurcation of the plume seen in many observed cases of wildland fires and other sources of buoyancy;
(2) The shear-layer (i.e. transverse) vortices that arise from a Kelvin–Helmholtz type instability on the upstream face of the plume; and
(3) The vertically oriented wake vortices that form with alternating sign and regular period in the lee of and beneath the bent-over plume.

These simulations also suggest that the degree to which the plume bifurcates is related to the depth of the cross-flow shear layer (a property also of the plumes arising from the realistic heat source), and that the periodicity of the wake vortices is linked to a periodic oscillation of the plume bifurcation in

which each branch of the bifurcation is successively dominant; however, more analysis is required in this regard to further characterize these simulated features.

The simulated plumes arising from the realistic heat source exhibit vortical structures that, although related to those seen in association with the circular source, are configured in a dramatically different manner. In particular, counter-rotating vortex pairs oriented in the streamwise direction form along each flank of the heat source, and transverse horizontal vortices form above the head of the heat source. The results of these simulations compare favorably with observations of plumes in wildland fires (e.g. Haines and Smith 1987).

The results presented in this paper have broad relevance to the dynamics of buoyant plumes in a cross flow, and the primary purpose of this paper is to illustrate the potential utility of numerical models to explore these phenomena. A considerable amount of additional analysis is now required to be able to draw firm conclusions about the detailed dynamical nature of the structure and evolution in these cases, particularly with respect to the identification of parameters that can be used to describe and characterize the flow over a wide range of conditions. Nevertheless, the present results are highly encouraging, and highlight many avenues for future research.

Finally, it is important to note that none of the simulated plumes shown in this paper displays a Gaussian cross-section; nor indeed have we seen Gaussian cross-sections in any of our simulations. Moreover, initial attempts to calculate and characterize the time-mean properties of the plume (not shown) have not yielded Gaussian structure either. Although the presence of bifurcation in the plume does not appear to affect plume rise significantly, it can be expected to play a critical role in smoke transport and dispersion, as may the other types of vortices seen in the simulations. The manner in which these vortical structures affect the transport and dispersion of smoke is not immediately apparent and requires further study, but the absence of self-similar Gaussian structure in the simulations shown here would appear to call into question the common practice of using plume rise and dispersion models that are based on these assumptions. From the perspective of the transport of particulate matter, the updrafts found along the centerline of the plume associated with the counter-rotating vortex pair may be strong enough to keep fine particles with small terminal velocities airborne long enough to prevent them from being deposited with a maximum concentration along the centerline, but instead they may be transported downward by the counter-rotating vortex pair on the flanks of the plume. In cases where the plume bifurcates, the majority of particles may be channeled into one of the branches. Such internal plume circulations might possibly lead to different distributions between particulate matter of different sizes (e.g. between PM2.5 and PM10 larger than 2.5 μm), and as such it is conceivable that present models are providing inaccurate predictions of the transport of fine particulate matter. With respect to the wake vortex system, it is of interest to examine the possibility that pollutants can be entrained from the plume into the wake downstream and beneath it via these vortices, leading potentially to localized but large instantaneous concentrations of smoke at the surface.

In light of the foregoing discussion, we suggest that an important aspect of future research is to assess the applicability of traditional plume models that assume a self-similar Gaussian structure, and to use a numerical model such as that described herein to explore alternative strategies for simplified plume modeling.

Acknowledgements

We thank two anonymous reviewers for constructive comments that clarified the presentation of our results. This research was partially supported by the USDA Forest Service, through a cooperative agreement with the USDA Forest Service Southern Research Station, and by the FSU School of Computational Science and Information Technology, through a grant of resources on the IBM SP Series 690 Power4-based supercomputer 'Eclipse'. This is contribution number 443 of the Geophysical Fluid Dynamics Institute at the Florida State University.

References

Banta RM, Olivier LD, Holloway ET, Kropfli RA, Bartram BW, Cupp RE, Post MJ (1992) Smoke column observations from two forest fires using Doppler lidar and Doppler radar. *Journal of Applied Meteorology* **31**, 1328–1349. doi:10.1175/1520-0450(1992)031<1328:SCOFTF>2.0.CO;2

Batchelor GK (1967) 'An introduction to fluid dynamics.' (Cambridge University Press: Cambridge)

Baum HR, McGrattan KB (2000) Simulation of large industrial outdoor fires. In 'Fire safety science. Proceedings of the sixth international symposium', Poitiers, France. pp. 611–622. (International Association for Fire Safety Science: Boston)

Briggs GA (1975) Plume rise predictions. In 'Lectures on air pollution and environmental impact analysis'. (Ed. DA Haugen) pp. 59–111. (American Meteorological Society: Boston)

Brown AR, Hobson JM, Wood N (2001) Large-eddy simulation of neutral turbulent flow over rough sinusoidal ridges. *Boundary-Layer Meteorology* **98**, 411–441. doi:10.1023/A:1018703209408

Church CR, Snow JT, Dessens J (1980) Intense atmospheric vortices associated with a 1000 MW fire. *Bulletin of the American Meteorological Society* **61**, 682–694. doi:10.1175/1520-0477(1980)061<0682:IAVAWA>2.0.CO;2

Clark TL, Jenkins MA, Coen JL, Packham DR (1996*a*) A coupled atmosphere–fire model: convective feedback on fire line dynamics. *Journal of Applied Meteorology* **35**, 875–901. doi:10.1175/1520-0450(1996)035<0875:ACAMCF>2.0.CO;2

Clark TL, Jenkins MA, Coen JL, Packham DR (1996*b*) A coupled atmosphere–fire model: role of the convective Froude number and dynamic fingering at the fireline. *International Journal of Wildland Fire* **6**, 177–190.

Coelho SLV, Hunt JCR (1989) The dynamics of the near field of strong jets in cross-flows. *Journal of Fluid Mechanics* **200**, 95–120.

Coleman GN (1999) Similarity statistics from a direct numerical simulation of the neutrally stratified planetary boundary layer. *Journal of the Atmospheric Sciences* **56**, 891–900. doi:10.1175/1520-0469(1999)056<0891:SSFADN>2.0.CO;2

Cortelezzi L, Karagozian AR (2001) On the formation of the counter-rotating vortex pair in transverse jets. *Journal of Fluid Mechanics* **446**, 347–373.

Deardorff JW (1973) The use of subgrid transport equations in a three-dimensional model of atmospheric turbulence. *Journal of Fluids Engineering* **95**, 429–438.

Fric TF, Roshko A (1994) Vortical structure in the wake of a transverse jet. *Journal of Fluid Mechanics* **279**, 1–47.

Haines DA, Smith MC (1987) Three types of horizontal vortices observed in wildland mass and crown fires. *Journal of Climate and Applied Meteorology* **26**, 1624–1637. doi:10.1175/1520-0450(1987)026<1624:TTOHVO>2.0.CO;2

Heilman WE, Fast JD (1992) Simulations of horizontal roll vortex development above lines of extreme surface heating. *International Journal of Wildland Fire* **2**, 55–68.

Hussaini MY (1998) On large-eddy simulation of compressible flows. AIAA Paper AIAA-1998–2802. (American Institute of Aeronautics and Astronautics: Reston)

Janseen LHJM, Nieuwstadt FTM, Donze M (1990) Time scales of physical and chemical processes in chemically reactive plumes. *Atmospheric Environment* **24A**, 2861–2874.

Lim TT, New TH, Luo SC (2001) On the development of large-scale structures of a jet normal to a cross flow. *Physics of Fluids* **13**, 770–775. doi:10.1063/1.1347960

Linn RR, Reisner JM, Colman JJ, Winterkamp J (2002) Studying wildfire behavior using FIRETEC. *International Journal of Wildland Fire* **11**, 233–246. doi:10.1071/WF02007

Luti FM (1980) Transient flow development due to a strong heat-source in the atmosphere. I. Uniform temperature source. *Combustion Science and Technology* **23**, 163–175.

Luti FM (1981) Some characteristics of a two-dimensional starting mass fire with cross flow. *Combustion Science and Technology* **26**, 25–33.

Margason RJ (1993) Fifty years of jet in crossflow research. In 'Proceedings of the AGARD symposium on computational and experimental assessment of jets in crossflow', Winchester, UK. (Advisory Group for Aerospace Research and Development: London)

Margolin LG, Smolarkiewicz PK, Wyszogrodzki AA (2002) Implicit turbulence modeling for high Reynolds number flows. *Journal of Fluids Engineering* **124**, 862–867. doi:10.1115/1.1514210

McGrattan KB, Baum HR, Rehm RG (1996) Numerical simulation of smoke plumes from large oil fires. *Atmospheric Environment* **30**, 4125–4136. doi:10.1016/1352-2310(96)00151-3

McRae DJ, Flannigan MD (1990) Development of large vortices on prescribed fires. *Canadian Journal of Forest Research* **20**, 1878–1887.

Moeng C-H, Rotunno R (1990) Vertical-velocity skewness in the buoyancy-driven boundary layer. *Journal of the Atmospheric Sciences* **47**, 1149–1162. doi:10.1175/1520-0469(1990)047<1149:VVSITB>2.0.CO;2

Moeng C-H, Wyngaard JC (1988) Spectral analysis of large-eddy simulations of the convective boundary layer. *Journal of the Atmospheric Sciences* **45**, 3573–3587. doi:10.1175/1520-0469(1988)045<3573:SAOLES>2.0.CO;2

Morton BR, Ibbetson A (1996) Jets deflected in a crossflow. *Experimental Thermal and Fluid Science* **12**, 112–133. doi:10.1016/0894-1777(95)00097-6

Morton BR, Taylor GI, Turner JS (1956) Turbulent gravitational convection from maintained and instantaneous sources. *Proceedings of the Royal Society of London A* **234**, 1–23.

Orlanski I (1976) A simple boundary condition for unbounded hyperbolic flows. *Journal of Computational Physics* **21**, 251–269. doi:10.1016/0021-9991(76)90023-1

Perry AE, Lim TT (1978) Coherent structures in coflowing jets and wakes. *Journal of Fluid Mechanics* **88**, 451–463.

Porterie B, Loraud JC, Morvan D, Larini M (1999) A numerical study of buoyant plumes in cross-flow conditions. *International Journal of Wildland Fire* **9**, 101–108. doi:10.1071/WF00001

Rudman M (1996) Simulation of the near field of a jet in a cross flow. *Experimental Thermal and Fluid Science* **12**, 134–141. doi:10.1016/0894-1777(95)00089-5

Schumann U (1991) Subgrid length-scales for large-eddy simulation of stratified turbulence. *Theoretical and Computational Fluid Dynamics* **2**, 279–290. doi:10.1007/BF00271468

Skamarock WC, Klemp JB, Dudhia J (2001) Prototypes for the WRF (Weather Research and Forecasting) model. In 'Preprints, ninth conference on mesoscale processes'. pp. J11–J15. (American Meteorological Society: Boston)

Slawson PR, Csanady GT (1967) On the mean path of buoyant, bent-over chimney plumes. *Journal of Fluid Mechanics* **28**, 311–322.

Soma S, Saito K (1991) Reconstruction of fire whirls using scale models. *Combustion and Flame* **86**, 269–284. doi:10.1016/0010-2180(91)90107-M

Trelles J, McGrattan KB, Baum HR (1999) Smoke transport by sheared winds. *Combustion Theory and Modelling* **3**, 323–341. doi:10.1088/1364-7830/3/2/307

Weil JC (1988) Plume rise. In 'Lectures on air pollution modeling'. (Eds A Venkatram, JC Wyngaard) pp. 119–166. (American Meteorological Society: Boston)

Wicker LJ, Skamarock WC (2002) Time-splitting methods for elastic models using forward time schemes. *Monthly Weather Review* **130**, 2088–2097. doi:10.1175/1520-0493(2002)130<2088:TSMFEM>2.0.CO;2

Wood VT (1992) Whirlwind formation at a burning oil supertanker in the Gulf of Mexico. *Monthly Weather Review* **120**, 371–372. doi:10.1175/1520-0493(1992)120<0371:WFAABO>2.0.CO;2

Yuan LL, Street RL (1998) Trajectory and entrainment of a round jet in crossflow. *Physics of Fluids* **10**, 2323–2335. doi:10.1063/1.869751

Yuan LL, Street RL, Ferziger JH (1999) Large-eddy simulations of a round jet in crossflow. *Journal of Fluid Mechanics* **379**, 71–104. doi:10.1017/S0022112098003346

Zhang X, Ghoniem AF (1993) A computational model for the rise and dispersion of wind-blown, buoyancy-driven plumes—I. Neutrally stratified atmosphere. *Atmospheric Environment* **15**, 2295–2311.